Biosensors and Bioelectronics 228 (2023) 115219

Contents lists available at ScienceDirect

Biosensors and Bioelectronics

journal homepage: www.elsevier.com/locate/bios

AgInZnS quantum dots as anodic emitters with strong and stable electrochemiluminescence for biosensing application

Zhuoxin Ye [a], Yibing Liu [a], Meichen Pan [b], Xiuli Tao [b], Yuxuan Chen [a], Pinyi Ma [a,**], Ying Zhuo [b,***], Daqian Song [a,*]

[a] College of Chemistry, Jilin Province Research Center for Engineering and Technology of Spectral Analytical Instruments, Jilin University, Qianjin Street 2699, Changchun, 130012, China

[b] Key Laboratory of Luminescence Analysis and Molecular Sensing (Southwest University), Ministry of Education, College of Chemistry and Chemical Engineering, Southwest University, Chongqing, 400715, China

ARTICLE INFO

Keywords:
Electrochemiluminescence
AgInZnS quantum dots
Biosensor
MicroRNA-141
Anodic emitters

ABSTRACT

Quantum dots (QDs) have become promising electrochemiluminescence (ECL) emitters with high quantum yield and size-tunable luminescence. However, most QDs generate strong ECL emission at the cathode, developing anodic ECL-emitting QDs with excellent performance is challenging. In this work, low-toxic quaternary AgInZnS QDs synthesized by a one-step aqueous phase method were used as novel anodic ECL emitters. AgInZnS QDs exhibited strong and stable ECL emission and a low excitation potential, which could avoid the side reaction of oxygen evolution. Furthermore, AgInZnS QDs displayed high ECL efficiency (Φ_{ECL}) of 5.84, taking the Φ_{ECL} of $Ru(bpy)_3^{2+}$/tripropylamine (TPrA) ECL system as 1. Compared to $AgInS_2$ QDs without Zn doping and traditional anode luminescent CdTe QDs, the ECL intensity of AgInZnS QDs was 1.62 times and 3.64 times higher than that of $AgInS_2$ QDs and CdTe QDs, respectively. As a proof-of-concept, we further designed an "on-off-on" ECL biosensor for detecting microRNA-141 based on a dual isothermal enzyme-free strand displacement reaction (SDR), which not only to achieve the cyclic amplification of the target and ECL signal, but also to construct a switch of the biosensor. The ECL biosensor had a wide linear range from 100 aM to 10 nM with a low detection limit of 33.3 aM. Together, the constructed ECL sensing platform is a promising tool for rapid and accurate diagnosis of clinical diseases.

1. Introduction

Electrochemiluminescence (ECL) is a bioanalytical technique that combines high controllability of electrochemical analysis with high sensitivity of luminescence analysis, and has been applied in a wide variety of biological detection(Fang et al., 2022; Qin et al., 2019; Zhao et al., 2020). Quantum dots (QDs) are ideal ECL emitters due to their unique optical properties of size-tunable luminescence, narrow emission peaks, high quantum yield, and good chemical stability (Ma et al., 2015; Wu et al., 2017; Xue et al., 2020). However, most luminescent QDs used as ECL emitters are binary II−VI and III–V QDs containing highly toxic elements, such as Cd, Pb and Hg (Lei et al., 2018; Pons et al., 2010). Recently, it has been reported that ternary I-III-VI QDs (I = Cu or Ag, III = Ga or In, and VI = S or Se) are promising alternatives because ternary QDs not only have favorable photoelectric properties similar to those of binary QDs, but also have low toxicity and are environmentally friendly (Deng et al., 2013; Zhong et al., 2012). Zou's group reported a facile route for synthesizing high-quality $CuInS_2$ nanocrystals (Chen et al., 2012). However, bare ternary QDs generally have surface defects/trap states, which will affect their luminescent properties and charge transfer. It has been shown that doping with transition metal ions can improve the performance of QDs (Jo et al., 2016; Li et al., 2022; You et al., 2022). To further improve the performance of ternary QDs, a new facile strategy is the synthesis of quaternary Zn−I−III−VI QDs. Liu and co-workers proposed a novel biosensor based on quaternary CuInZnS QDs as an ECL emitter (Liu et al., 2018a). According to the literature, most of the QDs exhibit cathodic ECL in the presence of the coreactants H_2O_2 or $S_2O_8^{2-}$. An extraordinarily negative potential is a prerequisite

* Corresponding author.
** Corresponding author.
*** Corresponding author.
E-mail addresses: mapinyi@jlu.edu.cn (P. Ma), yingzhuo@swu.edu.cn (Y. Zhuo), songdq@jlu.edu.cn (D. Song).

https://doi.org/10.1016/j.bios.2023.115219
Received 16 January 2023; Received in revised form 27 February 2023; Accepted 7 March 2023
Available online 8 March 2023

required to trigger strong ECL emission of cathodic luminescent QDs and may lead to the occurrence of hydrogen evolution side reaction and damage to biological activity of target (Dong et al., 2014; Gu et al., 2022; Mei et al., 2010). It is desirable to generate ECL emission of QDs at anodic potential to avoid the above adverse effects. However, only a few anodic ECL-emitting QDs have been reported, and the ECL intensity of these QDs (e.g., CdTe QDs (Liu and Ju, 2008) and CdSe QDs (Jiang and Wang, 2009)) is very weak. Therefore, developing anodic luminescent QDs with strong ECL emission is significant. The construction of quaternary Zn−I−III−VI QDs provides a promising way to prepare anodic luminescent materials.

MicroRNA-141 (miRNA-141) is considered as a potential tumor marker owing to its abnormal expression in breast cancer, prostate cancer, and other cancers (Bartel, 2004; Martins et al., 2022; Xu et al., 2017; Yin et al., 2012). However, it is challenging to sensitively detect miRNAs due to their ultralow abundance and high similarity to other miRNA members in the family (Ji et al., 2021; Li et al., 2019). To improve the detection sensitivity, several enzyme-assisted signal amplification strategies have been proposed, such as rolling circle amplification (RCA) (Wang et al., 2019), strand displacement amplification (SDA) (Chen et al., 2015) and loop-mediated isothermal amplification (LAMP) (Tang et al., 2019). The amplification efficiency of these enzyme-dependent methods can be affected by reaction conditions and activities of enzymes. Strand displacement reaction (SDR) is an enzyme-free and isothermal amplification process that can solve the above problems. This reaction is driven by the increase in the entropy of the system, instead of the enthalpy released by new base-pair formation, to convert the three-stranded DNA complex into a double-stranded waste complex, making the reaction irreversible (Lv et al., 2015; Zhang et al., 2018). Yang's group used SDR amplification to release the signal probe to amplify the target, but did not further amplify the ECL signal (Yu et al., 2021). Herein, we proposed a dual entropy-driven SDR, which allows for the cyclic amplification of the target and ECL signal to significantly improve sensitivity. This efficient and enzyme-free amplification strategy provides a favorable approach for miRNA detection.

In this study, using AgInZnS QDs as anodic ECL emitters and triethylamine (TEA) as a coreactant, a novel ECL biosensor for miRNA-141 detection was constructed combining with a dual entropy-driven SDR. As shown in Scheme 1A, AgInZnS QDs were synthesized by a one-step aqueous phase method. Then, QDs were immobilized on the electrode to generate strong ECL emission at the anodic potential with the aid of binder chitosan (CS). As shown in Scheme 1B, in the presence of the target miRNA-141, the first SDR was triggered as a result of the hybridization between the target and the exposed toehold of three-strand complexes (L-AP-MT), leading to the output of mimic target (MT), thus achieving amplification of the target. Subsequently, we constructed an ECL biosensing platform (Scheme 1C). Tetrahedral DNA nanostructure (TDN) that can reduce non-specific adsorption and can help adjust the distance between probes was assembled on the electrode modified by QDs as a capture probe, which hybridized with ferrocene-labeled probes (S1, S2), causing the signal to be in an "off" state. The obtained MT activated the second cycle of SDR, thus S1 and S2 were respectively released, causing the signal to be an "on" state. As expected, the above mechanisms allowed the ECL biosensor to have high selectivity and stability, as well as low detection limit. The designed biosensor was thus successfully applied to sensitively detect miRNA-141.

2. Experimental section

2.1. Synthesis of AgInZnS QDs

AgInZnS QDs were synthesized via a one-step method reported in the literature (Liu et al., 2021). Firstly, MPA (0.2 M, 5 mL), $AgNO_3$ (0.05 M, 0.2 mL), $In(ac)_3$ (0.05 M, 2 mL), and $Zn(ac)_2$ (0.05 M, 1 mL) were added into a 100 mL three-neck flask. The pH of the solution was adjusted to 9.5 using NaOH aqueous solution, followed by the addition of $Na_2S{\cdot}9H_2O$ (0.2 M, 2 mL) solution. The mixture was heated to 100 °C and then refluxed for 4.5 h. After cooling down to room temperature, the solution was centrifuged to remove unreacted materials, and the precipitate was discarded. The supernatant containing AgInZnS QDs was precipitated with EtOH and then centrifuged. Finally, pure QDs were obtained by vacuum drying.

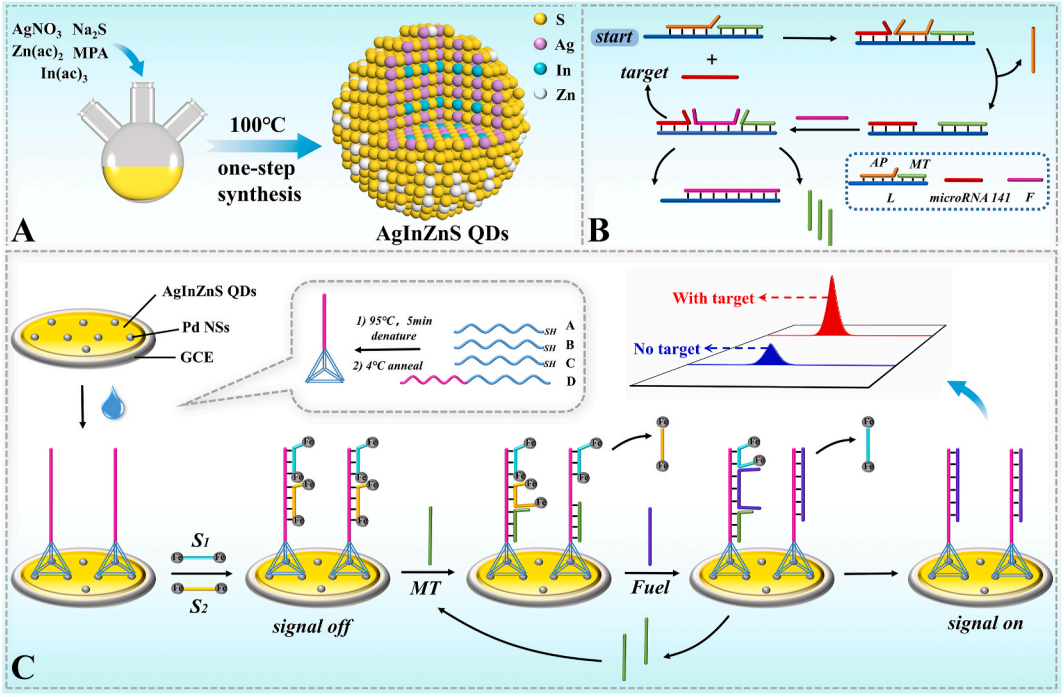

Scheme 1. Schematic illustration of the designed ECL biosensor for sensitive detection of target miRNA-141 via TDN-modified sensing platform.

2.2. Assembly of TDN and strand displacement reaction (SDR)

TDN was prepared by the annealing method (Xu et al., 2016). Before use, thiol-modified DNA strands were treated with TCEP (0.5 M) at 37 °C for 30 min to prevent the formation of disulfide bonds (Lu et al., 2019). First, equimolar amounts of four strands (A, B, C, D) were mixed with TM buffer to a final concentration of 1 μM (the optimal concentration of TDN was shown in Figure S6 (A)). Then, the mixture was heated to 95 °C for 10 min and then rapidly cooled down to 4 °C to allow stable TDN to form.

The steps in SDR were as follows. First, a mixture solution containing L, AP, and MT (all 3 μM) was prepared in Tri-HCl buffer. The mixture was annealed at 95 °C for 10 min and then slowly cooled down to room temperature to form L-AP-MT. Afterwards, different concentrations of target miRNA-141 (10 nM, 1 nM, 100 pM, 10 pM, 1 pM, 100 fM, 10 fM, 1 fM, and 100 aM) and F were reacted with L-AP-MT at 37 °C for 2 h. Ultimately, the product containing single-strand MT was stored in a refrigerator at 4 °C until further use.

2.3. Fabrication of biosensor

A bare glassy carbon electrode (GCE) was polished with 0.3- and 0.05-μm alumina powder in the respective order and then sonicated in ethanol and ultrapure water. Initially, 10 μL of AgInZnS QDs solution (0.5 mg/mL) containing 0.2% CS was dropped onto GCE. After drying, 10 μL of palladium nanospheres (Pd NSs) solution was dropped on the electrode and then dried. Then, 8 μL of TDN solution was added onto the modified electrode (GCE/AgInZnS QDs (CS)/Pd NSs) and incubated overnight at room temperature to immobilize TDN via Pd-S bonds (Jiang et al., 2019). Finally, 8 μL of a mixed solution containing S1 and S2 (each at 2.5 μM, the optimal concentrations of S1 and S2 were shown in Figure S6 (B)) was dropped onto the electrode (GCE/AgInZnS QDs (CS)/Pd NSs/TDN) and incubated for 2 h at 37 °C to obtain the biosensor (GCE/AgInZnS QDs (CS)/Pd NSs/TDN/S1, S2).

2.4. Procedures for ECL measurement

The ECL measurement was carried out as follows. First, 8 μL of a mixture containing MT (SDR product) and Fuel (3 μM) was incubated with the ECL biosensor for 2 h at 37 °C. The biosensor was then rinsed with ultrapure water to remove unreacted MT and Fuel. After that, in 2 mL of PBS containing 10 μL of TEA, the ECL signal was measured by a three-electrode system using an MPI-E ECL analyzer. The potential was scanned from −0.3 to 1.1 V at a scanning rate of 0.3 V/s.

2.5. Polyacrylamide gel electrophoresis (PAGE)

The analysis of the SDR product was carried out by PAGE. DNA samples were mixed with the loading buffer (volume ratio = 5:1) and then loaded onto a 20% polyacrylamide gel. The electrophoresis was carried out at 120 V for 1.5 h. The formation of TDN was confirmed by 12% polyacrylamide gel, of which the electrophoresis was performed at 120 V for 80 min.

3. Results and discussion

3.1. Morphology characterization of AgInZnS QDs

The morphology of AgInZnS QDs was characterized by transmission electron microscopy (TEM). Fig. 1A showed that QDs had a uniform spherical morphology and good monodispersity with an average size of 4.7 nm. Fig. 1B showed the clear lattice of AgInZnS QDS with a lattice distance of 0.21 nm, indicating the high-quality crystallinity of QDs. X-ray diffraction (XRD) of AgInZnS QDs was performed for further phase confirmation. Three diffraction peaks of QDs matched with (002), (110), and (112) phases of the hexagonal structure (Fig. S1, Supporting Information). In addition, energy-dispersive spectrometry (EDS) analysis (Fig. S2) showed Ag, Zn, In, S, and C signals, confirming that QDs were composed of Ag, In, Zn, and S (C and excess S were produced by MPA agent).

3.2. Optical properties of AgInZnS QDs

The 3D surface image (Fig. 1C) and heat map (Fig. 1D) of AgInZnS QDs containing TEA as a coreactant showed that the maximum ECL emission was 590 nm. The luminescence potential was 1.1 V, which was below the oxygen evolution potential (1.79 V vs. Ag/AgCl) of GCE modified by AgInZnS QDs, an indication that there was no side reaction

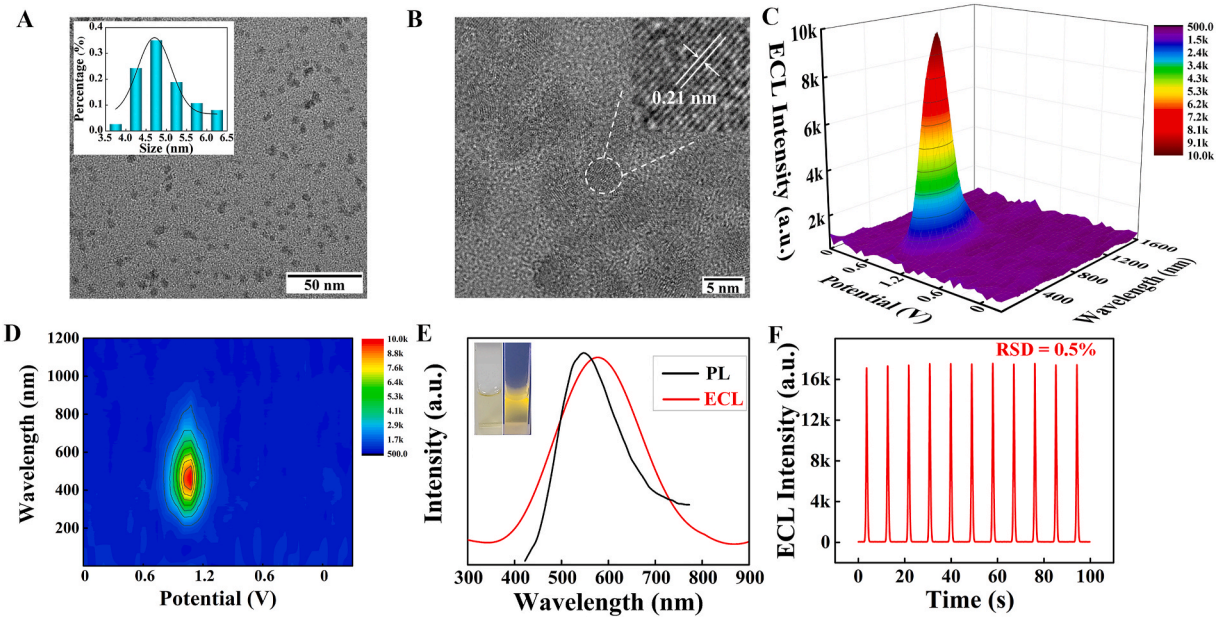

Fig. 1. (A) TEM images of AgInZnS QDs at 50-nm scale. The inset shows the size distribution of AgInZnS QDs. (B) TEM images of AgInZnS QDs at 5-nm scale. (C) 3D surface image and (D) heat map of AgInZnS QDs in PBS solution containing TEA. (E) Comparison of PL and ECL spectrum of AgInZnS QDs (the inset shows the images of AgInZnS QDs under visible light (left) and UV light (right)). (F) Stability of AgInZnS QDs after 11 cycles of continuous scanning.

of oxygen evolution (Supporting Information, Fig. S4). Fig. 1E depicted the photoluminescence (PL) and ECL spectra of AgInZnS QDs. At an excitation wavelength of 400 nm, the maximum PL emission wavelength of the material was 550 nm. In addition, the inset of Fig. 1E presented that the material appeared pale yellow color under visible light and bright yellow luminescence under a 365-nm UV lamp. The ECL emission spectrum of AgInZnS QDs closely resembled that of the PL spectrum, with a slight red-shift by only 40 nm, due to the passivation of QDs surface (Jiang and Wang, 2009). The ECL stability of AgInZnS QDs was depicted in Fig. 1F. There was no significant fluctuation in ECL intensity after 11 cycles of continuous scanning, and the relative standard deviation (RSD) was only 0.5%. This indicates that AgInZnS QDs have excellent ECL stability.

The luminescence intensity and stability of $AgInS_2$ QDs without Zn doping were measured. As shown in Fig. 2A, the luminescence intensity of AgInZnS QDs (17313 a.u.) was 1.62 times that of $AgInS_2$ (10709 a.u.), which was attributed to the change in luminescence properties caused by Zn doping. AgInZnS is an I-type core-shell semiconductor QDs, which is characterized by a larger band gap of the shell material than the band gap of the core. Most of the $AgInS_2$ QDs possessed an energy gap (E_g) about 1.87eV. The ZnS nanoparticles is about 3.65eV. The synthesis process in this work belongs to "particle coating". The coating formed by doping Zn can passivate surface ion defects and reduce the probability of non-radiative transitions, thus increasing the ECL intensity of the QDs (Liu et al., 2018b; Torimoto et al., 2007). The ECL intensity and stability of AgInZnS QDs were further compared with those of the reported anodic luminescent QDs, including classical luminophores CdTe QDs and low-toxic MoS_2 QDs, as shown in Fig. 2B and Fig. S5, respectively. The ECL intensity of AgInZnS QDs was 3.64 times and 8.07 times higher than that of CdTe QDs (4750 a.u.) and MoS_2 QDs (2145 a.u.), respectively. In addition, through several cycles of continuous scanning, the stability of AgInZnS QDs (RSD = 0.5%) was found to be the highest among all these QDs (Fig. 2C, D, and S5). Moreover, when the ECL efficiency (Φ_{ECL}) of $[Ru(bpy)_3]^{2+}$/tripropylamine (TPrA) system was taken as 1, AgInZnS QDs exhibited high Φ_{ECL} of 5.84 (the details are shown in Supporting Information). These comparisons reveal that AgInZnS QDs have superior luminescence performance.

3.3. Polyacrylamide gel electrophoresis analysis of TDN and SDR

To demonstrate the successful assembly of TDN, gel electrophoresis was performed. As shown in Fig. 3A, each of the four strands used for assembling the TDN, A (lane 1), B (lane 2), C (lane 3), and D (lane 4), appeared as a single band. Bands in lanes 5 and 6 represented the hybridization of two strands (A + B) and three strands (A + B + C), respectively; and compared to these bands, band for TDN (lane 7) had slower mobility, confirming that the assembly of TDN was successful. In addition, the absence of by-product in band 7 indicates the high hybridization efficiency to generate TDN. PAGE was also employed to verify the generation of SDR product (Fig. 3B). Only a single band was observed in lane 1, indicating that the hybridization product of L, AP and MT, L-AP-MT, was successfully formed. MT appeared as a single band in lane 5 and did not appear in lane 2 (F + L-AP-MT). This suggests that MT cannot be displaced with F in the absence of miRNA-141, indicating that this strategy does not generate false positive signals. When miRNA-141 and F were added to L-AP-MT (lane 3), a new band of MT emerged. Compared with that in lane 1, L-AP-MT band in lane 3 disappeared and a lower band of the hybridization product of L and F appeared. Lane 4 represents the hybridization product of L and F. The above results suggest that the occurrence of the proposed nucleic amplification.

3.4. Possible ECL mechanism of the proposed ECL system

To validate the ECL reaction mechanism of AgInZnS QDs, ECL and CV measurements were carried out. As shown in Figure S7 (A), low ECL signals were detected in GCE modified with AgInZnS QDs in PBS solution (curve a) and in bare GCE in PBS solution containing TEA (curve b).

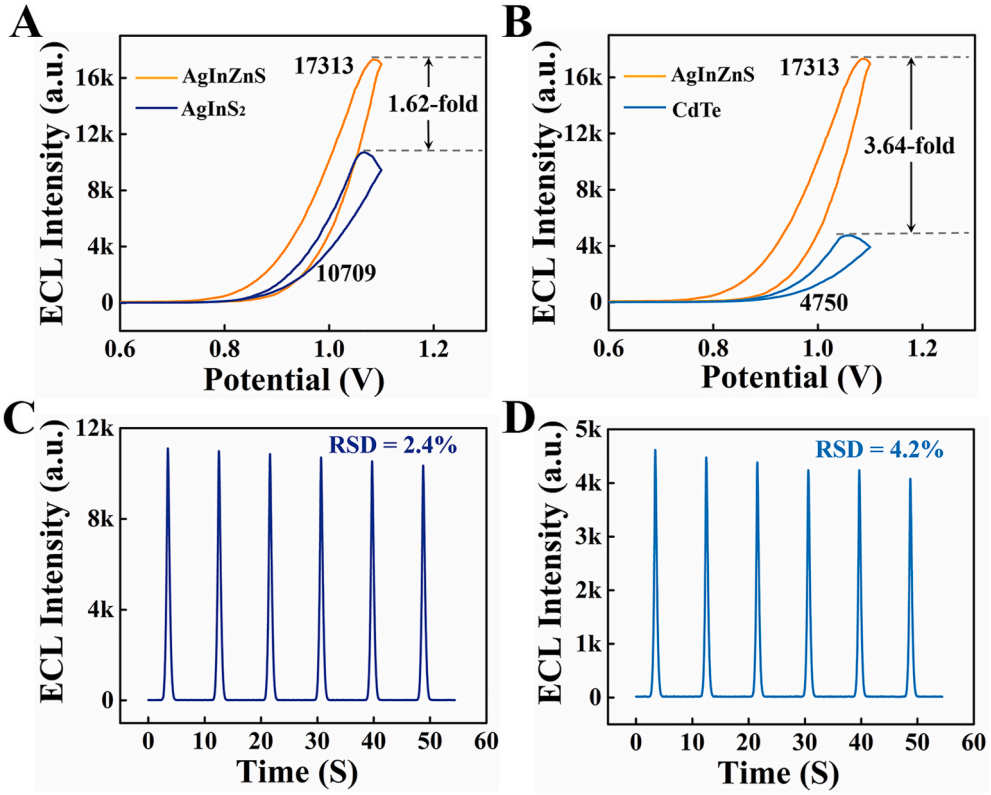

Fig. 2. ECL intensity of $AgInS_2$ QDs (A), CdTe QDs (B). ECL stability of $AgInS_2$ QDs (C), CdTe QDs (D).

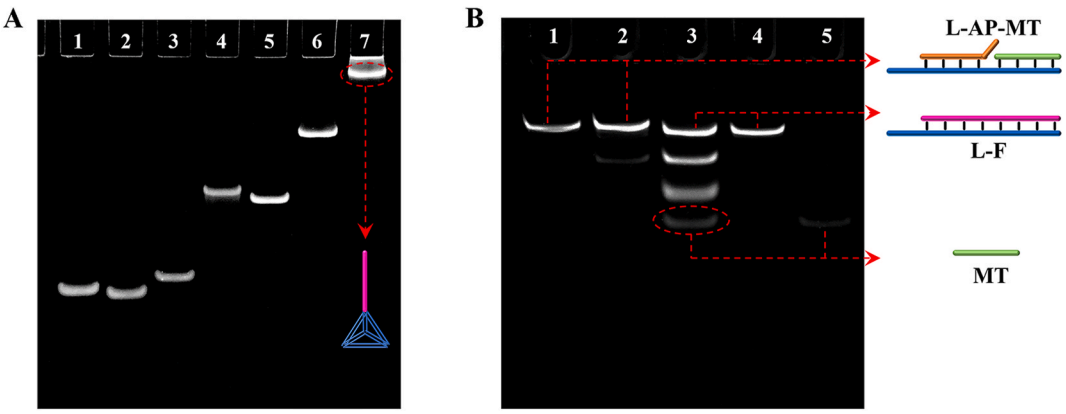

Fig. 3. (A) PAGE analysis of TDN (lanes 1–4: A, B, C and D (each at 1 μM), lane 5: A + B (each at 1 μM), lane 6: A + B + C (each at 1 μM), and lane 7: A + B + C + D (each at 1 μM)). (B) PAGE analysis of SDR product (lane 1: L + MT + AP (each at 1 μM), lane 2: L + MT + AP + F (each at 1 μM), lane 3: L + MT + AP (each at 1 μM) + miRNA-141 (2 μM) + F (2 μM), lane 4: L + F (each at 1 μM), and lane 5: MT (1 μM)).

Meanwhile, the corresponding CV curves (Figure S7 (B), curve a and b) showed a low current. However, in the presence of the coreactant TEA, the ECL signal of AgInZnS QDs was significantly enhanced (Figure S7 (A), curve c) and the current was increased (Figure S7 (B), curve c). In the CV curve, curves a and c have a weak oxidation peak at 0.75 V, which was obtained by the oxidation of the AgInZnS QDs. TEA can lose its electrons to form a strong reductant $TEA^{\bullet}$ that can reduce AgInZnS QDs^{+} to its excited state (AgInZnS QDs*), which after returning to its ground state can produce intense ECL emission. A possible ECL reaction mechanism of AgInZnS QDs is as follows:

$$\text{AgInZnS QDs} + e^{-} \rightarrow \text{AgInZnS QDs}^{+}$$

$$\text{TEA} + e^{-} \rightarrow \text{TEAH}^{+\bullet}$$

$$\text{TEAH}^{+\bullet} \rightarrow \text{TEA}^{\bullet} + H^{+}$$

$$\text{AgInZnS QDs}^{+} + \text{TEA}^{\bullet} \rightarrow \text{AgInZnS QDs*} + \text{products}$$

$$\text{AgInZnS QDs*} \rightarrow \text{AgInZnS QDs} + h\nu\ (590\ \text{nm})$$

3.5. Characterization of the modified electrode

The feasibility of ECL biosensor in an experiment was verified. As can be seen in Fig. 4A, when AgInZnS QDs were modified onto the electrode in the presence of TEA coreactant (curve a), a remarkable ECL signal of 17313 a.u. was achieved. After adding Pd NSs, the signal of the AgInZnS QDs remained almost unchanged (curve b). Subsequently, in the presence of the assembled TDN (curve c), the ECL signal decreased, due to the obstruction of electron transfer by TDN. When a mixture of S1 and S2 was incubated with the electrode (curve d), the ECL signal was quenched due to the quenching effect of ferrocene (Cao et al., 2006). Finally, the ECL intensity partially recovered (curve e) after a mixture of MT (the SDR product of 100 nM target) and Fuel was incubated with the modified GCE, which allowed for the release of S1 and S2.

The assembly process of the biosensor was characterized by cyclic voltammetry (CV). As shown in Fig. 4B, a pair of redox peaks of $[Fe(CN)_6]^{3-/4-}$ could be observed in the CV curve for bare GCE (curve a). When AgInZnS QDs were modified onto GCE, the current increased significantly (curve b) because of the excellent conductivity of AgInZnS QDs. However, after TDN was assembled on the electrode (curve c), the redox peak currents decreased, due to the blockage of electron transfer by TDN. Then, after a mixture of S1 and S2 was incubated with the electrode (curve d), the redox peak current decreased. Finally, when a mixture containing MT and Fuel was dropped onto the electrode, the redox peak currents decreased due to the repulsion effect between $[Fe(CN)_6]^{3-/4-}$ and negatively charged double-stranded DNA (Liu et al., 2017). Altogether, these characterization results indicated that the biosensor was successfully fabricated.

3.6. ECL performance of the biosensor

The performance of the proposed biosensor was investigated by employing it to quantitatively detect miRNA-141 at different concentrations. As displayed in Fig. 5A and B, the ECL intensity increased gradually with increasing concentration of miRNA-141. In addition, the increment of ECL intensity (ΔI_{ECL}) had a good liner relationship with the logarithm of miRNA-141 concentration ranging from 100 aM to 10 nM (Fig. 5C). The linear regression equation was $\Delta I_{ECL} = 15004.27 + 893.5$

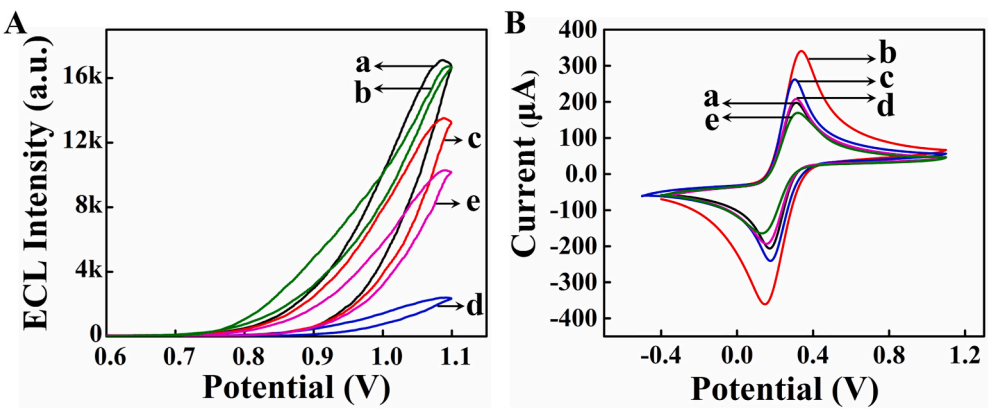

Fig. 4. (A) ECL intensity-potential curves at each assembly step of biosensor: (a) GCE/AgInZnS QDs (CS); (b) GCE/AgInZnS QDs (CS)/Pd NSs; (c) GCE/AgInZnS QDs (CS)/Pd NSs/TDN; (d) GCE/AgInZnS QDs (CS)/Pd NSs/TDN/S1, S2; and (e) GCE/AgInZnS QDs (CS)/Pd NSs/TDN/S1, S2/MT, Fuel. (B) CV curves measured in $[Fe(CN)_6]^{3-/4-}$ solution: (a) GCE; (b) GCE/AgInZnS QDs (CS); (c) GCE/AgInZnS QDs (CS)/Pd NSs/TDN; (d) GCE/AgInZnS QDs (CS)/Pd NSs/TDN/S1, S2; and (e) GCE/AgInZnS QDs (CS)/Pd NSs/TDN/S1, S2/MT, Fuel.

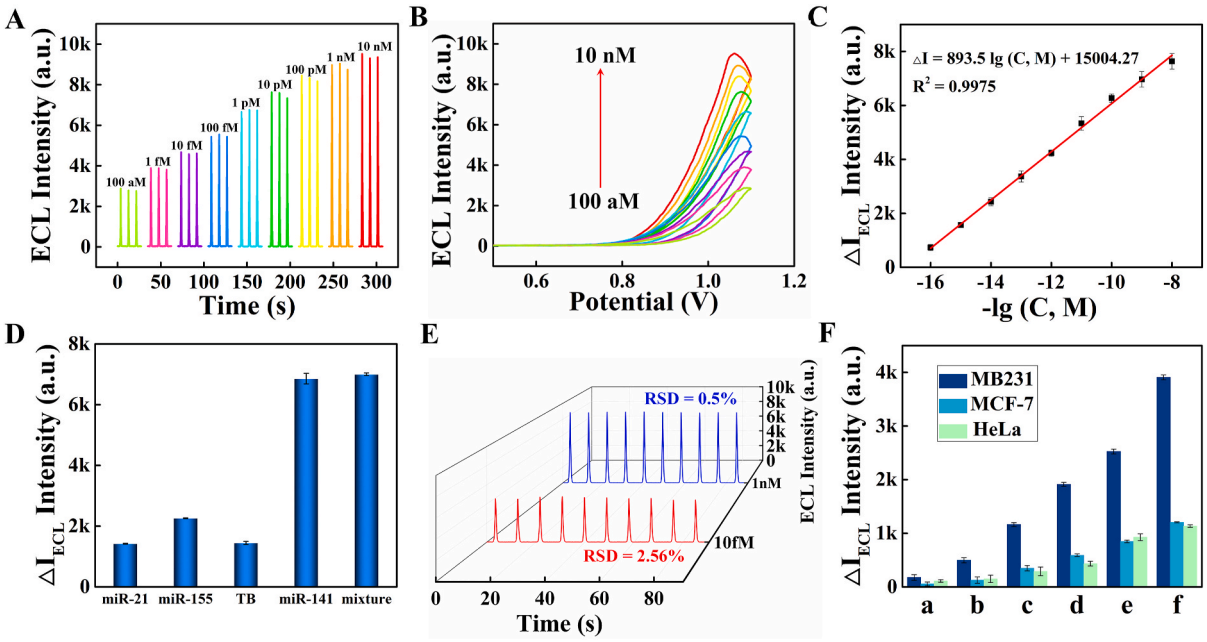

Fig. 5. (A) ECL responses of the proposed biosensor in the presence of miRNA-141 at different concentrations. (B) ECL intensity-potential curves of the biosensor incubated with miRNA-141 at different concentrations. (C) Calibration plot showing the linear relationship between ΔI_{ECL} and the logarithm of miRNA-141 concentration (n = 3). The RSD of the linear plots from 100 aM to 10 nM were 3.9%, 1.5%, 3.3%, 3.7%, 1.8%, 3.4%, 1.8%, 3.1%, 2.9%. (D) Selectivity of the proposed ECL biosensor toward different types of miRNAs. Concentration of all interfering miRNAs was 1 nM, and that of the target miRNA-141 was 100 nM. The RSD were 0.35%, 0.27%, 1.3%, 1.9%, 0.48% respectively. (E) Stability of the proposed ECL biosensor in the presence of miRNA-141 at concentrations of 10 fM and 1 nM. (F) Detection of miRNA-141 by the ECL biosensor in MB231, MCF-7 and HeLa cells at varying amounts of (a) 5, (b) 5×10^1, (c) 5×10^2, (d) 5×10^3, (e) 5×10^4, and (f) 5×10^5 cells.

lgC with a correlation coefficient of 0.9975. The limit of detection (LOD) was 33.3 aM at a signal-to-noise ratio (S/N) of 3. Compared with other strategies reported in the literature, the proposed biosensor had higher analytical performance in miRNA-141 detection; it had a wider linear range and a lower detection limit. The comparison between the performance of the biosensor presented in this work and that of other reported miRNA-141 detection methods is listed in Table S2 (Supporting Information).

3.7. Stability and selectivity of the ECL biosensor

The performance of the biosensor, in terms of selectivity and stability, was further evaluated. To assess the selectivity, miRNA-21, miRNA-155 and thrombin (TB) were employed as interferences in comparative experiments. As shown in Fig. 5D, the significant ΔI_{ECL} was observed only in the presence of miRNA-141 (1 nM). However, in the presence of miRNA-21, miRNA-155 and TB (100 nM), the ΔI_{ECL} was slightly increased but remained much lower than that in the presence of miRNA-141. The ΔI_{ECL} of a mixture containing the three interferences (100 nM) and miRNA-141 (1 nM) was nearly the same as that of miRNA-141 alone. These results demonstrate that the proposed biosensor had satisfactory selectivity towards miRNA-141.

Besides, the stability of the biosensor was examined by subjecting it to continuous scanning for 10 cycles and then using it to detect 10 fM and 1 nM miRNA-141. As displayed in Fig. 5E, the RSD in detecting 10 fM and 1 nM miRNA-141 was 2.56% and 0.50%, respectively, indicating that the biosensor has satisfactory stability.

3.8. Detection of miRNA-141 in human serums

The applicability of the designed biosensor in real human serum samples was evaluated by a standard addition method. The samples were prepared by spiking different concentrations of miRNA-141 (10 nM, 100 pM, 1 pM, and 10 fM) into real serum samples from healthy individuals. As shown in Table S3, the recoveries of miRNA-141 in human serum samples ranged from 95.8% to 103%, suggesting that the proposed biosensor can detect miRNA-141 in real human samples and can potentially be applied in the clinical detection of miRNA-141.

3.9. Detection of miRNA-141 in different tumor cells

The applicability of the biosensor in detecting miRNA-141 in cell lysates of MB231, MCF-7, and HeLa cells was further evaluated. As depicted in Fig. 5F, with increasing amount of MB231 cells from 5 to 5×10^5 cells, the ECL signal increased significantly. However, with increasing amount of MCF-7 and HeLa cells from 5 to 5×10^5 cells, the ECL signal increased slowly and was slower than the increase caused by MB231 cells. These results demonstrate that the expression level of miRNA-141 in MB231 cells is higher than that in MCF-7 and HeLa cells. The above finding is consistent with the observation reported in the literature (Xia et al., 2019; Yin et al., 2012).

4. Conclusions

To sum up, an "on-off-on" ECL miRNA-141 detection biosensor was successfully constructed based on the quaternary AgInZnS QDs synthesized by a one-step aqueous phase method as novel anodic ECL emitters. AgInZnS QDs exhibited a strong and stable ECL emission at the anode and high Φ_{ECL} of 5.84. In addition, a dual isothermal enzyme-free SDR was introduced into the biosensor system. The cyclic amplification of the target and the construction of biosensor "off-on" switch could be realized through SDR. Based upon these advantages, the developed ECL biosensor had a wide linear response and a low detection limit of as low as 33.3 aM. Besides, the biosensor also had excellent stability and selectivity. It was successfully applied to detect miRNA-141 in real human serum and tumor cells with satisfactory results. Altogether, this work not only opens up new frontiers for the design and construction of efficient ECL materials, but also provides a new strategy for the accurate

and rapid detection of cancer marker miRNAs.

CRediT authorship contribution statement

Zhuoxin Ye: Conceptualization, Data curation, Formal analysis, Investigation, Writing – original draft. **Yibing Liu:** Data curation, Investigation. **Meichen Pan:** Formal analysis, Investigation. **Xiuli Tao:** Data curation, Investigation. **Yuxuan Chen:** Literature summary, Investigation. **Pinyi Ma:** Conceptualization, Project administration, Data curation, Writing – review & editing. **Ying Zhuo:** Investigation, Resources, Writing – review & editing. **Daqian Song:** Project administration, Funding acquisition, Resources, Supervision.

Declaration of competing interest

The authors declare that they have no known competing financial interests or personal relationships that could have appeared to influence the work reported in this paper.

Data availability

Data will be made available on request.

Acknowledgments

This work was supported by the National Natural Science Foundation of China (22004046 and 22074052).

Appendix A. Supplementary data

Supplementary data to this article can be found online at https://doi.org/10.1016/j.bios.2023.115219.

References

Bartel, D.P., 2004. Cell 116 (2), 281–297.
Cao, W., Ferrance, J.P., Demas, J., Landers, J.P., 2006. J. Am. Chem. Soc. 128 (23), 7572–7578.
Chen, A., Gui, G.F., Zhuo, Y., Chai, Y.Q., Xiang, Y., Yuan, R., 2015. Anal. Chem. 87 (12), 6328–6334.
Chen, B., Zhong, H., Zhang, W., Tan, Z.a., Li, Y., Yu, C., Zhai, T., Bando, Y., Yang, S., Zou, B., 2012. Adv. Funct. Mater. 22 (10), 2081–2088.
Deng, D., Qu, L., Zhang, J., Ma, Y., Gu, Y., 2013. ACS Appl. Mater. Interfaces 5 (21), 10858–10865.
Dong, Y.P., Gao, T.T., Zhou, Y., Zhu, J.J., 2014. Anal. Chem. 86 (22), 11373–11379.
Fang, Y., Hou, Y., Yang, H., Chen, R., Li, W., Ma, J., Han, D., Cao, X., Liu, S., Shen, Y., Zhang, Y., 2022. Adv. Opt. Mater. 10 (18), 2201017.
Gu, W., Wang, X., Xi, M., Wei, X., Jiao, L., Qin, Y., Huang, J., Cui, X., Zheng, L., Hu, L., Zhu, C., 2022. Anal. Chem. 94 (26), 9459–9465.
Ji, K., Wang, Y., Mao, L., Wang, Y., Zhang, X., 2021. Sensor. Actuator. B Chem. 345, 130405.
Jiang, H., Wang, X.-M., 2009. Electrochem. Commun. 11 (6), 1207–1210.
Jiang, M.H., Li, S.K., Zhong, X., Liang, W.B., Chai, Y.Q., Zhuo, Y., Yuan, R., 2019. Anal. Chem. 91 (5), 3710–3716.
Jo, D.Y., Kim, D., Kim, J.H., Chae, H., Seo, H.J., Do, Y.R., Yang, H., 2016. ACS Appl. Mater. Interfaces 8 (19), 12291–12297.
Lei, Y.M., Zhou, J., Chai, Y.Q., Zhuo, Y., Yuan, R., 2018. Anal. Chem. 90 (20), 12270–12277.
Li, F., Benetti, D., Zhang, M., Shi, L., Feng, J., Wei, Q., Rosei, F., 2022. ACS Appl. Mater. Interfaces 14 (49), 54790–54802.
Li, Y., Huang, C.Z., Li, Y.F., 2019. Anal. Chem. 91 (14), 9308–9314.
Liu, J.L., Tang, Z.L., Zhuo, Y., Chai, Y.Q., Yuan, R., 2017. Anal. Chem. 89 (17), 9108–9115.
Liu, X., Ju, H., 2008. Anal. Chem. 80 (14), 5377–5382.
Liu, Y., Chen, X., Ma, Q., 2018a. Biosens. Bioelectron. 117, 240–245.
Liu, Y., Tang, X., Deng, M., Zhu, T., Bai, Y., Qu, D., Huang, X., Qiu, F., 2018b. J. Lumin. 202, 71–76.
Liu, Y., Tang, X., Deng, M., Zhu, T., Edman, L., Wang, J., 2021. J. Alloys Compd. 864, 158109.
Lu, J., Wang, J., Hu, X., Gyimah, E., Yakubu, S., Wang, K., Wu, X., Zhang, Z., 2019. Anal. Chem. 91 (11), 7353–7359.
Lv, Y., Cui, L., Peng, R., Zhao, Z., Qiu, L., Chen, H., Jin, C., Zhang, X.B., Tan, W., 2015. Anal. Chem. 87 (23), 11714–11720.
Ma, M.N., Zhuo, Y., Yuan, R., Chai, Y.Q., 2015. Anal. Chem. 87 (22), 11389–11397.
Martins, C.S.M., LaGrow, A.P., Prior, J.A.V., 2022. ACS Sens. 7 (5), 1269–1299.
Mei, Y.-L., Wang, H.-S., Li, Y.-F., Pan, Z.-Y., Jia, W.-L., 2010. Electroanalysis 22 (2), 155–160.
Pons, T., Pic, E., Lequeux, N., Cassette, E., Bezdetnaya, L., Guillemin, F., Marchal, F., Dubertret, B., 2010. ACS Nano 4 (5), 2531–2538.
Qin, D., Jiang, X., Mo, G., Feng, J., Yu, C., Deng, B., 2019. ACS Sens. 4 (2), 504–512.
Tang, Z., Choi, G., Nouri, R., Guan, W., 2019. Nano Lett. 19 (11), 7927–7934.
Torimoto, T., Adachi, T., Okazaki, K., Sakuraoka, M., Shibayama, T., Ohtani, B., Kudo, A., Kuwabata, S., 2007. J. Am. Chem. Soc. 129 (41), 12388–12389.
Wang, J., Wang, H., Wang, H., He, S., Li, R., Deng, Z., Liu, X., Wang, F., 2019. ACS Nano 13 (5), 5852–5863.
Wu, F.-F., Zhou, Y., Wang, J.-X., Zhuo, Y., Yuan, R., Chai, Y.-Q., 2017. Sensor. Actuator. B Chem. 243, 1067–1074.
Xia, L.Y., Zheng, Y.N., Liang, W.B., Li, M.J., Hu, T., Yuan, R., Chai, Y.Q., 2019. Chem. Eur J. 25 (16), 4087–4092.
Xu, F., Dong, H., Cao, Y., Lu, H., Meng, X., Dai, W., Zhang, X., Al-Ghanim, K.A., Mahboob, S., 2016. ACS Appl. Mater. Interfaces 8 (49), 33499–33505.
Xu, Z., Liao, L., Chai, Y., Wang, H., Yuan, R., 2017. Anal. Chem. 89 (16), 8282–8287.
Xue, S., Jiang, X.F., Zhang, G., Wang, H., Li, Z., Hu, X., Chen, M., Wang, T., Luo, A., Ho, H.P., He, S., Xing, X., 2020. ACS Sens. 5 (4), 1002–1009.
Yin, B.C., Liu, Y.Q., Ye, B.C., 2012. J. Am. Chem. Soc. 134 (11), 5064–5067.
You, Y., Tong, X., Channa, A.I., Li, X., Liu, C., Ye, H., Wang, Z., 2022. EcoMat 4 (5), e12206.
Yu, L., Zhu, L., Yan, M., Feng, S., Huang, J., Yang, X., 2021. Anal. Chem. 93 (34), 11809–11815.
Zhang, N., Shi, X.M., Guo, H.Q., Zhao, X.Z., Zhao, W.W., Xu, J.J., Chen, H.Y., 2018. Anal. Chem. 90 (20), 11892–11898.
Zhao, T., Zhou, Q., Lv, Y., Han, D., Wu, K., Zhao, L., Shen, Y., Liu, S., Zhang, Y., 2020. Angew. Chem. Int. Ed. 59 (3), 1139–1143.
Zhong, H., Bai, Z., Zou, B., 2012. J. Phys. Chem. Lett. 3 (21), 3167–3175.